Universitat
de les Illes Balears

Cluster Crystals under an external flow

MARTÍN E. MAZA-CUELLO

Master**'s** Thesis

Master's degree in Physics of Complex Systems

at the

UNIVERSITAT DE LES ILLES BALEARS

Academic year 2017 - 2018

July 2018

UIB Master's Thesis Supervisor: Cristóbal López Sánchez

UIB Master's Thesis Co-Supervisor: Emilio Hernández-García

Abstract

Brownian particles interacting via a purely repulsive, soft-core pairwise potential can arrange themselves into a stable hexagonal lattice where each site is occupied by a cluster of overlapping particles, known as a "Cluster Crystal". This occurs only when the potential has negative Fourier components and the diffusion is sufficiently low. In this Master Thesis, we perturb this stable pattern by adding an external shear flow to the dynamics. Using a direct simulation of the particles' motion, we show that the flow promotes the formation of channels of clusters parallel to the flow direction, with the clusters travelling along them. These channels are separated in the transversal direction by a distance that seems independent of the flow strength. This scale, together with the separation between the clusters inside a channel, is of the order of the lattice constant of the static hexagonal pattern. The inter-channel distance is mainly controlled by the interaction length of the potential. Increasing the diffusion coefficient allows the particles to jump from a channel to another and expand the clusters, but does not affect their transversal periodicity. The critical value of the diffusion is also not altered by the presence of the flow, for the set of values investigated. By pursuing a linear stability analysis of the Dean-Kawasaki equation, with the addition of the external flow, we are able to qualitatively explain the results obtained from the simulations. Finally, we briefly discuss some effects of applying an alternating flow.

Acknowledgements

To the IFISC staff, who makes possible this Master. To my supervisors, Cristóbal and Emilio, for their guidance and critical comments. To my classmates, for their sympathy and insights. To my parents, Diego and Paulina, for their example of effort and perseverance. To Raquel, for her kind and patient company.

Thank you.

Agradecimientos

Al personal del IFISC, que hace posible este Máster. A mis supervisores, Cristóbal y Emilio, por su guía y comentarios críticos. A mis compañeros, por su simpatía y sugerencias. A mis padres, Diego y Paulina, por su ejemplo de esfuerzo y perseverancia. A Raquel, por su alegre y paciente compañía.

Muchas gracias.

Contents

Chapter 1

Introduction

The concept of soft matter, developed during the second half of the 20th century, provides a general scenario for studying the behaviour of mesoscopic particles dispersed in different solvent media. Liquid crystals, colloids, or even polymer chains are well-known examples of complex fluids [2], which represent a relevant topic with direct industrial and pharmaceutical applications [10]. There has been also a growing interest in applying these concepts to some biological systems on small scales, which have been encompassed under the name of soft "active" matter [11]. The term "soft" captures the idea that these systems are extremely sensitive to external parameters compared to atomic or molecular materials where structural changes induced by external forcing are linear for small deformations [8, 10].

It is precisely this sensitivity what allows the existence of a rich variety of particles interactions in soft matter systems, that may strongly depend even on the shape of the particles (e.g. it depends on whether they are rigid but polydisperse, or formed by elastic chains, or are star-shaped) [8]. A broad diversity of phase transitions, spatiotemporal structures and driven complex phases both in equilibrium and non-equilibrium scenarios therefore emerges [8, 10, 11]. The need of a theoretical explanation for these phenomena and the description of their underlying mechanisms led to the development of a field-theoretical approach inspired on models of pure fluids and their equilibrium properties [8]. As a result, effective interactions between particles capturing different aspects of the soft matter

peculiarities have been characterized [8].

Recently, attention has been devoted to systems of particles interacting via an effective soft-core potential, which allows overlapping between them [4,7,12,13,15]. Importantly, it has been shown that even purely repulsive potentials can induce a Liquid-Solid transition and the formation of crystal-like structures for sufficiently high densities [4, 9, 12, 13], when the potentials are bounded and have negative Fourier components [7] (for a full proof based on Density Functional Theory, see Ref. [9]). A further question in this type of system has been the effect of a linear shear applied on the boundaries, studied in 3D cells [15]. Under this condition, the particles aggregate forming columns of overlapping particles that follow the flow, forming a hexagonal structure in the transversal plane [15]. The primary focus of these works has been on the influence of the pattern on the viscosity and stresses along the system [15].

The emergence of ordered spatiotemporal patterns in this scenario has been studied in detail recently by J.-B. Delfau *et al.* [4], for the generalized exponential model (GEM-α) with interaction potential $V(\mathbf{x}) = \varepsilon \exp(-|\mathbf{x}/R|^{\alpha})$ [4, 12]. In their work, using numerical simulations of the Brownian dynamics in 1D and 2D cells, accompanied with the theoretical framework provided by the Dean-Kawasaki equation [3,4], they showed that this aggregation phenomena appears only if some of the negative Fourier components of the interaction potential overcome the diffusion, and they computed the critical values of the diffusion coefficient and the associated lattice constant for different GEM-α potentials by means of a linear stability analysis. Those modes generate an instability over the homogeneous state (the one intuitively expected for diffusive, repulsive particles) which eventually generates a freezing transition into a regular hexagonal pattern. This hexagonal lattice is formed by clusters of overlapping particles, which are repelled by neighbouring clusters via an effective interaction mechanism [4]. The lattice constant therefore depends on the leading (negative) modes of the potential [4].

In this Master Thesis, we extend the investigation on cluster crystals by analysing (in a two-dimensional geometry) the cluster formation process when an external

flow is superimposed to the dynamics of the particles. In Chapter 2, we present the main tools used in this work, explaining the derivation of the Dean-Kawasaki equation for the dynamics of the density of particles [1,3], used latter for the theoretical discussion, together with the simulation methods and the relevant control parameters investigated. The interaction potential and the flow used for this project are also discussed. Afterwards, in Chapter 3, we present our main results about the effects of applying an external steady flow to the system. We study the effects of changing the flow intensity, the diffusion coefficient and the interaction length, and compare the resulting pattern with the previous work by J.-B. Delfau *et al.* [4]. A qualitatively justification of the results obtained in the simulations, following a similar linear stability analysis as the one applied in the static case in Ref. [4], is provided in the final section. A further scenario is briefly covered in Chapter 4 when the external flow is alternating, presenting features of chaotic mixing. The conclusions and possible future extensions of this work are finally discussed in Chapter 5.

Chapter 2

Main tools

In this Master Thesis, we have employed a direct numerical simulation of the dynamics of the particles together with a theoretical description of the model in terms of the dynamics of the system's density of particles. The computational approach gives information about the actual trajectories and interactions between the particles and how they stay on, or leave the spatiotemporal patterns that emerge in the system. These structures are collective modes of the system, and their emergence and dynamics are better understood using a field description which points out which are the relevant parameters that control the behaviour of the system.

2.1 Brownian dynamics with external flow

We will consider a system of N interacting particles driven by an external flow $\mathbf{u}(\mathbf{x}, t)$, defined by the system of Langevin coupled equations

$$\begin{cases} \dot{\mathbf{x}}_i = \mathbf{v}_i & (2.1) \\ m\dot{\mathbf{v}}_i = -\gamma\left[\mathbf{v}_i - \mathbf{u}(\mathbf{x}_i, t)\right] + F_{int}(\mathbf{x}_i) + \sqrt{2\gamma k_B T}\boldsymbol{\xi}_i(t), & (2.2) \end{cases}$$

for $i = 1, 2, \ldots, N$, where m is the mass of the particles, $\boldsymbol{\xi}_i(t)$ are independent Gaussian vector noises of zero mean and correlations

$$\left\langle \boldsymbol{\xi}_i(t)\boldsymbol{\xi}_j(t')\right\rangle = \mathbb{I}\delta_{ij}\delta(t-t'), \tag{2.3}$$

and $F_{int}(\mathbf{x})$ is the force exerted by the particles due to a pairwise potential interaction. The external flow will be considered to be incompressible, $\nabla \cdot \mathbf{u}(\mathbf{x}, t) = 0$.

We will work in the overdamped limit, $m/\gamma \to 0$. The particles follow the Brownian dynamics [1]

$$\dot{\mathbf{x}}_i = -\sum_{j=1}^{N} \nabla_i V(\mathbf{x}_i - \mathbf{x}_j) + \mathbf{u}(\mathbf{x}_i, t) + \sqrt{2D}\boldsymbol{\xi}_i(t), \qquad i = 1, 2, \ldots, N \tag{2.4}$$

triggered by the interaction forces $F_{int}(\mathbf{x})/\gamma = -\sum_{j=1}^{N} \nabla V(\mathbf{x} - \mathbf{x}_j)$, where $V(\mathbf{x})$ is an interacting pairwise soft-core potential such that $\nabla V(0) = 0$, and the external forcing $\mathbf{u}(\mathbf{x}, t)$. The diffusion coefficient is given by the Einstein relation $D = k_B T/\gamma$ [4]. The Itô interpretation of (2.4) is used, in particular through the analytical discussion of Sec. 2.2, although the corresponding Stratonovich equation is the same due to the the noises being additive [1, 6, 16].

In later chapters we will perform direct simulations of the set of equations (2.4) to explore the different effects that the flow may produce on the clusters and the hexagonal pattern of the static case. To gain some insight about the mechanisms behind the emergence of collective structures we will need a description of the dynamics of the particle density of the system.

2.2 Dean-Kawasaki equation with external flow

The density dynamics is given by the Dean-Kawasaki equation, which exactly describes the time evolution of the density of our ensemble of interacting Brownian particles subjected to white noise in the overdamped regime [1, 3, 5], with the addition of an external forcing [1] that we will model as a flow driving the particles. We are going to derive this equation as was done in the original paper by Dean (see Ref. [3] for the derivation, and Refs. [1, 5] for a discussion on its meaning and mathematical justification).

Our aim is to construct a closed equation for the number density operator

[1, 3, 5]

$$\hat{\rho}(\mathbf{x},t) = \sum_{i=1}^{N} \hat{\rho}_i(\mathbf{x},t) \equiv \sum_{i=1}^{N} \delta(\mathbf{x}_i(t) - \mathbf{x}). \tag{2.5}$$

The derivation follows usual arguments from the theory of distributions.

Consider an arbitrary, well-behaved function $f(\mathbf{x})$ over the region of interest. From the definition of the single particle operators $\hat{\rho}_i(\mathbf{x},t)$, it follows that

$$f(\mathbf{x}_i(t)) = \int d\mathbf{x}\, \delta(\mathbf{x}_i(t) - \mathbf{x}) f(\mathbf{x}) = \int d\mathbf{x}\, \hat{\rho}_i(\mathbf{x},t) f(\mathbf{x}), \tag{2.6}$$

and therefore

$$\frac{df(\mathbf{x}_i(t))}{dt} = \int d\mathbf{x}\, f(\mathbf{x})\, \partial_t \hat{\rho}_i(\mathbf{x},t). \tag{2.7}$$

On the other hand, since $\mathbf{x}_i(t)$ is a stochastic process, the left hand side derivative can be performed using Itô Calculus [1, 3, 6], which gives

$$\begin{aligned}\frac{df(\mathbf{x}_i(t))}{dt} &= \nabla f(\mathbf{x}_i)\cdot\dot{\mathbf{x}}_i + D\nabla^2 f(\mathbf{x}_i) = \\ &= \int d\mathbf{x}\, \hat{\rho}_i(\mathbf{x},t)\times \\ &\quad \times \left[\nabla f(\mathbf{x})\cdot\left\{\sqrt{2D}\boldsymbol{\xi}_i(t) - \sum_{j=1}^{N}\nabla V(\mathbf{x}-\mathbf{x}_j(t)) + \mathbf{u}(\mathbf{x},t)\right\} + D\nabla^2 f(\mathbf{x})\right].\end{aligned} \tag{2.8}$$

Integrating by parts, we obtain

$$\begin{aligned}\frac{df(\mathbf{x}_i(t))}{dt} = \int d\mathbf{x}\, f(\mathbf{x})\Bigg[&- \sqrt{2D}\nabla\cdot\Big(\hat{\rho}_i(\mathbf{x},t)\boldsymbol{\xi}_i(t)\Big) + \nabla\cdot\left(\hat{\rho}_i(\mathbf{x},t)\sum_{j=1}^{N}\nabla V(\mathbf{x}-\mathbf{x}_j(t))\right) - \\ &- \nabla\cdot\Big(\hat{\rho}_i(\mathbf{x},t)\mathbf{u}(\mathbf{x},t)\Big) + D\nabla^2\hat{\rho}_i(\mathbf{x},t)\Bigg].\end{aligned} \tag{2.9}$$

Comparing now (2.7) and (2.9), we get the evolution of the single-particle operator,

$$\begin{aligned}&\partial_t\hat{\rho}_i(\mathbf{x},t) + \nabla\cdot\Big[\hat{\rho}_i(\mathbf{x},t)\mathbf{u}(\mathbf{x},t)\Big] = \\ &\quad = D\nabla^2\hat{\rho}_i(\mathbf{x},t) + \nabla\cdot\left[\hat{\rho}_i(\mathbf{x},t)\sum_{j=1}^{N}\nabla V(\mathbf{x}-\mathbf{x}_j(t))\right] - \sqrt{2D}\nabla\cdot\Big[\hat{\rho}_i(\mathbf{x},t)\boldsymbol{\xi}_i(t)\Big].\end{aligned} \tag{2.10}$$

We want to sum over all particles to get the evolution of the density operator $\hat{\rho}(\mathbf{x},t)$. To simplify the notation, let us define the summed Gaussian noise

$$\xi(\mathbf{x},t) = -\sqrt{2D}\sum_{i=1}^{N}\nabla\cdot\Big[\hat{\rho}_i(\mathbf{x},t)\boldsymbol{\xi}_i(t)\Big] \tag{2.11}$$

which can be shown to have mean zero and correlations [3]

$$\langle\xi(\mathbf{x},t)\xi(\mathbf{x}',t')\rangle = 2D\delta(t-t')\left[\nabla_{\mathbf{x}}\cdot\nabla_{\mathbf{x}'}\right]\Big(\delta(\mathbf{x}-\mathbf{x}')\hat{\rho}(\mathbf{x})\Big). \tag{2.12}$$

This noise can in turn be shown to be statistically equivalent to the multiplicative term [3]

$$\xi(\mathbf{x},t) \overset{\text{stat}}{=} \nabla\cdot\Big[\sqrt{2D\hat{\rho}(\mathbf{x},t)}\,\boldsymbol{\eta}(\mathbf{x},t)\Big] \tag{2.13}$$

where $\boldsymbol{\eta}(\mathbf{x},t)$ is another Gaussian white noise characterized by

$$\langle\boldsymbol{\eta}(\mathbf{x},t)\rangle = 0, \qquad \langle\boldsymbol{\eta}(\mathbf{x},t)\boldsymbol{\eta}(\mathbf{x}',t')\rangle = \mathbb{I}\delta(t-t')\delta(\mathbf{x}-\mathbf{x}'). \tag{2.14}$$

Noting furthermore that

$$\sum_{j=1}^{N}\nabla V(\mathbf{x}-\mathbf{x}_j(t)) = \sum_{j=1}^{N}\int d\mathbf{x}'\hat{\rho}_j(\mathbf{x}',t)\nabla V(\mathbf{x}-\mathbf{x}') = \int d\mathbf{x}'\hat{\rho}(\mathbf{x}',t)\nabla V(\mathbf{x}-\mathbf{x}'), \tag{2.15}$$

equation (2.10) is finally replaced by

$$\begin{aligned}\partial_t\hat{\rho}(\mathbf{x},t) + \nabla\cdot\Big[\hat{\rho}(\mathbf{x},t)\mathbf{u}(\mathbf{x},t)\Big] &= \nabla\cdot\left[\hat{\rho}(\mathbf{x},t)\int d\mathbf{x}'\hat{\rho}(\mathbf{x}',t)\nabla V(\mathbf{x}-\mathbf{x}')\right] + \\ &+ D\nabla^2\hat{\rho}(\mathbf{x},t) + \nabla\left[\sqrt{2D\hat{\rho}(\mathbf{x},t)}\,\eta(\mathbf{x},t)\right],\end{aligned} \tag{2.16}$$

which is the Dean-Kawasaki equation with an additional current term [1]. If the external flow is incompressible, $\nabla\cdot\mathbf{u}(\mathbf{x},t) = 0$, then equation (2.16) is equal to

$$\begin{aligned}\partial_t\hat{\rho}(\mathbf{x},t) + \Big(\mathbf{u}(\mathbf{x},t)\cdot\nabla\Big)\hat{\rho}(\mathbf{x},t) &= \nabla\cdot\left[\hat{\rho}(\mathbf{x},t)\int d\mathbf{x}'\hat{\rho}(\mathbf{x}',t)\nabla V(\mathbf{x}-\mathbf{x}')\right] + \\ &+ D\nabla^2\hat{\rho}(\mathbf{x},t) + \nabla\left[\sqrt{2D\hat{\rho}(\mathbf{x},t)}\,\eta(\mathbf{x},t)\right],\end{aligned} \tag{2.17}$$

where now the new term represents an advective contribution.

This equation, without the advective term, has been successfully applied in Ref. [4] to explain the emergence of cluster crystals, the conditions for the clusters

to form, and their effective interactions and approximate Gaussian shape. The addition of the advective term will be important to understand the results obtained from the simulations, and will be discussed at the end of Chapter 3 in Sec. 3.4. Before going into the simulations, however, it is important to understand which are the relevant parameters that control the behaviour of the system. These will be clear after nondimensionalizing expression (2.17).

2.3 Control parameters

To define the control parameters and to understand their meaning, it is useful to rewrite equation (2.17) in dimensionless form, rescaling the variables in view of the scales introduced by the interaction potential $V(\mathbf{x})$. In general, it seems reasonable to assume an interaction of the form

$$V(\mathbf{x}) = \varepsilon\, \tilde{V}\left(\frac{\mathbf{x}}{R}\right), \tag{2.18}$$

introducing the interaction's energy scale ε and length scale R. Let us note that a purely repulsive potential will have both $\varepsilon > 0$ and non-negative $\tilde{V}(\mathbf{x}/R)$. In the same way, we will assume that the flow has some characteristic velocity U, and that it can thus be written as $\mathbf{u}(\mathbf{x}, t) = U\, \boldsymbol{v}(\mathbf{x}, t)$.

The interaction scales are to be compared with those introduced by the diffusion and the advection terms. Using the mean density $\rho_0 = N/L^2$ to normalize $\hat{\rho}$, we define the dimensionless variables as

$$\tilde{\mathbf{x}} \equiv \frac{\mathbf{x}}{R}, \qquad \tilde{t} \equiv (\varepsilon \rho_0)\, t, \qquad \tilde{\rho}\left(\tilde{\mathbf{x}}, \tilde{t}\right) \equiv \frac{\hat{\rho}(\mathbf{x}, t)}{\rho_0}. \tag{2.19}$$

Equation (2.17) can now be rewritten as, dropping the tildes of $\tilde{\mathbf{x}}$ and $\tilde{t}$,

$$\begin{aligned}\partial_t \tilde{\rho}(\mathbf{x}, t) + \tilde{U}(\tilde{\boldsymbol{v}}(\mathbf{x}, t) \cdot \nabla)\tilde{\rho}(\mathbf{x}, t) =& \nabla \cdot \left[\tilde{\rho}(\mathbf{x}, t) \int d\mathbf{x}' \nabla \tilde{V}(|\mathbf{x}' - \mathbf{x}|)\tilde{\rho}(\mathbf{x}', t)\right] + \\ &+ \tilde{D}\nabla^2 \tilde{\rho}(\mathbf{x}, t) + \frac{1}{\sqrt{n_R}} \nabla \cdot \left[\sqrt{2\tilde{D}\tilde{\rho}(\mathbf{x}, t)}\, \boldsymbol{\eta}(\mathbf{x}, t)\right].\end{aligned} \tag{2.20}$$

The dimensionless parameters

$$\tilde{D} = \frac{D}{(\varepsilon \rho_0 R^2)}, \qquad \tilde{U} = \frac{U}{(\varepsilon \rho_0 R)}, \qquad n_R = \rho_0 R^2, \tag{2.21}$$

control the behaviour of the system. The first two parameters measure ratios between the typical time scales of different processes and the interaction timescale $\tau_{int} = 1/(\varepsilon\rho_0)$, inside an area $\sim R^2$. $\tilde{D}$ relates to the diffusive timescale $\tau_{diff} = R^2/D$, whereas $\tilde{U}$ defines the flow timescale $\tau_{flow} = R/U$. The third parameter, n_R, measures the number of particles in the typical interaction area, and reduces the fluctuations when the density is high.

2.4 Simulations

In this Master Thesis, we integrate numerically the system of coupled equations (2.4), restated here for clarity,

$$\dot{\mathbf{x}}_i = -\sum_{j=1}^{N} \nabla_i V(\mathbf{x}_i - \mathbf{x}_j) + \mathbf{u}(\mathbf{x}_i, t) + \sqrt{2D}\boldsymbol{\xi}_i(t), \qquad i = 1, 2, \ldots, N \tag{2.22}$$

where $\boldsymbol{\xi}_i(t)$ are independent Gaussian vector noises of zero mean and delta correlated.

For the soft-core interaction potential $V(\mathbf{x})$, we use the generalized exponential model GEM-3 potential [4, 12]

$$V(\mathbf{x}) = \varepsilon \exp\left(-\left|\frac{\mathbf{x}}{R}\right|^3\right), \tag{2.23}$$

which introduces the energy scale ε and the length scale R. As commented earlier, the family of GEM-α potentials have been shown to induce pattern formation if D is weak enough for $\alpha > 2$ in different dimensions [4, 12, 15]. The condition $\alpha > 2$ is necessary for the potential to have negative Fourier components [9, 12], which may overcome the diffusive transport [4]. The relation between these quantities will be explained at the end of Sec. 3.4 with the help of the Dean-Kawasaki equation (2.20) just derived.

Regarding the external flow $\mathbf{u}(\mathbf{x}, t)$, in Chapter 3 we will present our main results using a steady shear flow, whereas in Chapter 4 we will indicate some effects of using an alternating flow. In both cases, it will be based on the sine-flow

$$\mathbf{u}(\mathbf{x}, t) = \begin{cases} U \sin(qy + \phi)\, \hat{\mathbf{e}}_x & 0 < t \leq T/2 \\ U \sin(qx + \phi)\, \hat{\mathbf{e}}_y & T/2 < t \leq T \end{cases} \tag{2.24}$$

where t is taken mod T and $q = 2\pi/L$ is the wavenumber associated to the cell size. This kinematic flow is used in studies of chaotic advection and diffusion [14], as a toy model for studying mixing processes. The velocity field of the flow is shown in Fig. 2.1 for $\phi = 0$. The flow acts alternatively in two orthogonal directions, without any temporal modulation between the direction swifts. Although in Chapter 4 we will use the full expression, in Chapter 3 we focus on the effects of the steady shear flow $\mathbf{u}(\mathbf{x}) = U \sin(qy + \phi)\, \hat{\mathbf{e}}_x$ which corresponds to the first part of the sine-flow, equation (2.24), that is represented in the left panel of Fig. 2.1.

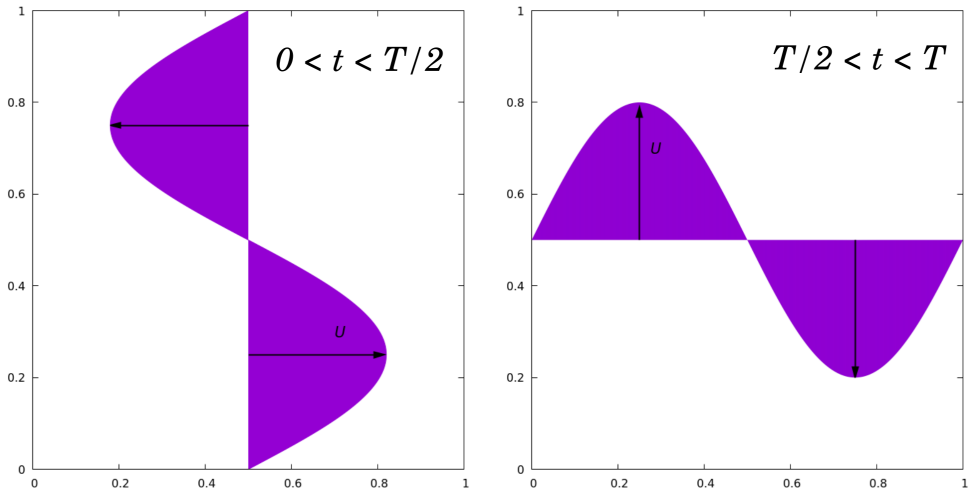

Figure 2.1: Velocity field profile of the sine-flow $\mathbf{u}(\mathbf{x}, t)$ profile given by equations (2.24) (left panel) and (2.24) (right panel) with $\phi = 0$. The time t is to be taken mod T. In Chapter 3 only the velocity field of the left panel will be used, while the complete oscillating flow will be used in Chapter 4.

Each simulation is initially set in a different random configuration. The set of equations (2.4) is integrated using the Heun algorithm [16] with time-step $h = 0.001$. We have checked for the set of parameters employed that the dynamics does not change if $h = 0.0001$ is taken instead. We will simulate the dynamics for

$N = 2000$ particles in a 2D square cell of length L, which is set to be the unity of length. Periodic boundary conditions are imposed in both directions.

In each section of the Chapter 3 we perform simulations by changing one the main parameters of the system: the flow strength $\tilde{U}$, the diffusion coefficient $\tilde{D}$ and the interaction length R. Our reference values will be $\tilde{U} = 3$, $\tilde{D} = 0.015$, and $R = 0.1L$ (which correspond to $n_R = 20$ particles in an interaction region). The values of $\tilde{D}$ and R were chosen following Ref. [4] to set the parameters in the clustering regime of the static case, with the interaction energy scale $\varepsilon = 0.0333$ which fixes the value of the interaction time to $\tau_{int} = 0.015$. Another important parameter will turn out to be the wavevector of the sine-flow, which in dimensionless form is $\tilde{q} \equiv qR = 2\pi R/L$. For $R = 0.1L$, its value is $\tilde{q} \approx 0.63$.

Chapter 3

Shear flow

We begin by studying the case of steady, shear flow. By taking expression (2.24) solely, we apply the external velocity field $\mathbf{u}(\mathbf{x}) = U \sin(qy)\, \hat{\mathbf{e}}_x$, which corresponds to the left panel of Fig. 2.1, without performing any direction swifts. We set $\phi = 0$, so that particles in the bottom half are driven by the flow to the right of the cell, and those in the upper half are driven to the left in our plots. By changing alternatively the flow strength $\tilde{U}$, the diffusion coefficient $\tilde{D}$ and the interaction length R, we explore the patterns that emerge.

3.1 Cluster formation dependence on $\tilde{U}$

Firstly, we have studied the system for several values of flow strength $\tilde{U}$, to compare the formation of clusters with the static ($\tilde{U} = 0$) case. Fig. 3.1 shows the evolution of the system for different values of $\tilde{U}$, with $\tilde{D} = 0.015$ and $R = 0.1L$, starting from different random initial conditions. It is important to bear in mind that these are particular snapshots and the clusters are moving with the velocity imposed by the flow, as reminded by the dashed lines superimposed on each configuration, and that the pattern is therefore not static. The flow does not inhibit the formation of clusters, although the hexagonal pattern of the static case ($\tilde{U} = 0$) is deformed and eventually disappears after a sufficiently long time.

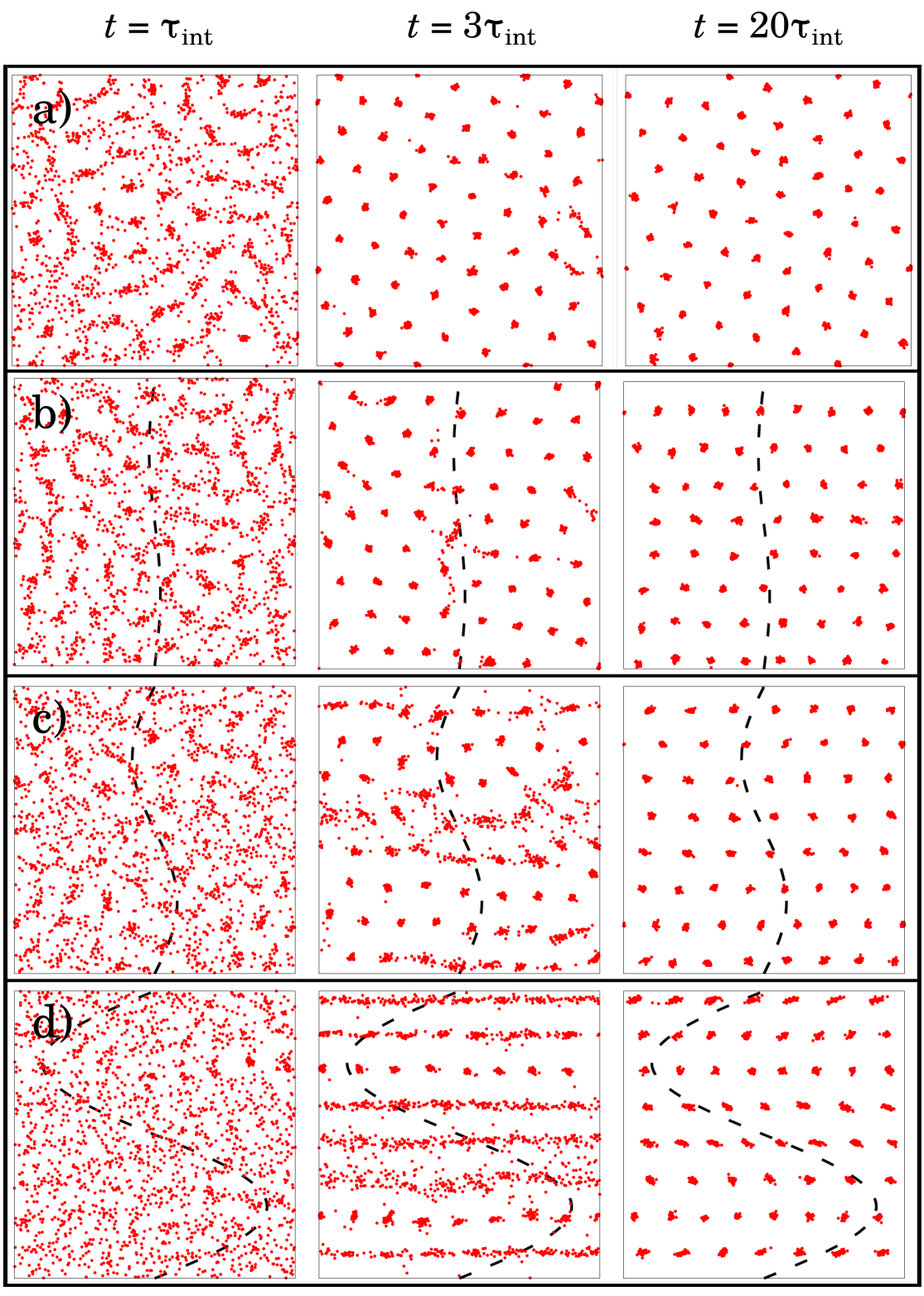

Figure 3.1: Typical particle configurations at different times for different velocities: a) static case, $\tilde{U} = 0$. b) $\tilde{U} = 0.75$, $\tau_{flow} = (4/3)\tau_{int}$. c) $\tilde{U} = 3$, $\tau_{flow} = (1/3)\tau_{int}$. d) $\tilde{U} = 15$, $\tau_{flow} = (1/15)\tau_{int}$ (integrated with an integration step of $h = 0.0002$ to improve resolution). Superimposed dashed curves are the sine-flow profiles, shown for clarity. The amplitudes of the curves on different rows are proportional to the ratios between the corresponding values of $\tilde{U}$.

From the snapshots at $t = 20\tau_{int}$ (last column), it is clear that the flow introduces a privileged direction which appears earlier as $\tilde{U}$ grows, as seen in Fig. 3.1d) when $\tilde{U} = 15$. Even in the case of small $\tilde{U}$, as in Fig. 3.1b) with $\tilde{U} = 0.75$, the pattern formed will organize itself following the flow direction after a sufficiently long time (same row, last snapshot $t = 20\tau_{int}$). Clusters at a particular height in the transversal direction move with the same speed, generating a structure of quasi-1D channels of clusters parallel to the direction of the flow, each one following to flow with a particular velocity. This structure is clearly seen in the second snapshot of Fig. 3.1d).

It is seen that channels appear before or after the formation of clusters depending on whether τ_{flow} is greater or lesser than τ_{int}, respectively. Let us recall that this relationship is measured by $\tilde{U}$, since $\tilde{U} = \tau_{int}/\tau_{flow}$. If we compare the different configurations of the first column of in Fig. 3.1, as $\tilde{U}$ increases the formation of clusters during the first τ_{int} interval seems to be hindered. When $\tilde{U} < 1$, as in Fig. 3.1b), clusters form first (first snapshot) and, after a transient process where the clusters rearrange their positions when driven by the flow (second snapshot), they order in longitudinal channels of clusters that move coherently with the flow velocity at that particular (transversal) height (third snapshot). On the contrary, when $\tilde{U} > 1$ as in Fig. 3.1c) and d), the flow slows down the formation of clusters while enhancing the rapid modulation of the density in the transversal direction (Fig. 3.1d), second snapshot).

It is also interesting the fact that the clusters appear earlier near the maxima of the sine-profile, whereas near its nodes the shear hinders the development of structures. This is specially clear in the middle area of the second snapshot of Fig. 3.1c), where neither clusters nor channels are defined whereas near the maxima of the profile channels of clusters have already appeared. This effect of the shear is also present in the last snapshot of Fig. 3.1d), where the clusters in the most upper channel are deformed following the flow profile, while those at the maxima are more regular. Finally, let us also note that not all the channels have the same number of clusters. This can be seen in the last configurations of Figs. 3.1b)–

d), some of the channels having 7 and others 8 clusters. We have followed these simulations until $t \sim 34\tau_{int}$ to see if these numbers had fluctuations, but this was not the case –each channel maintains its population of clusters.

Regardless the value of $\tilde{U}$, the same non-equilibrium steady state is reached. 8 channels of clusters are formed for these values of $\tilde{D}$ and R. To study the periodicity of the channels and compare it with the periodicity of the system without flow, we define the two-point distribution function

$$g^{(2)}(\mathbf{x}) = \frac{1}{\rho_0} \left\langle \sum_{i \neq 0} \delta(\mathbf{x} - \mathbf{x}_i) \right\rangle , \tag{3.1}$$

obtained in the simulations with a time average over at least 20 configurations separated a time interval Δt of the order of a few simulation steps, beginning from $t \sim 7\tau_{int}$ so as to reach the non-equilibrium steady state where the channels are already formed. (We have checked that results are essentially independent of the choice of Δt).

$g^{(2)}(\mathbf{x})$ measures the distribution of particles relative to the position of a reference particle $\mathbf{x}_0$. Fig. 3.2 compares $g^{(2)}(\mathbf{x})$ for $\tilde{U} = 0$ (static case) and $\tilde{U} = 15$, both with $\tilde{D} = 0.015$ and $R = 0.1L$. In the static case, Fig. 3.2a), the expected hexagonal structure emerges. From this figure, the intercluster distance of the static case is seen to be around $a^0 \simeq 1.4R/L$. This value is near the reference value $1.44R/L$ given in Ref. [4] at the critical point (i.e. the system with maximum value of $\tilde{D}$ at which the pattern is stable, see discussion in Sec. 3.4 below). In the case of $\tilde{U} = 15$, Fig. 3.2b), the average unveils the channels in which the clusters are ordered. The latter are washed out by the average, since clusters in different channels propagate with different velocities, which moreover are related via a non-linear relationship. The channel in the centre is the only one that preserves the clusters since these move coherently with the reference particle. Note that, apart from the middle one, the clusters of the central channel appear as blurred. This is a consequence of having channels with different number of clusters, as pointed out earlier. Besides, the central cluster appears slightly elongated in the longitudinal direction in Fig. 3.2b), as a consequence of the deformation of

the clusters by the shear as commented above.

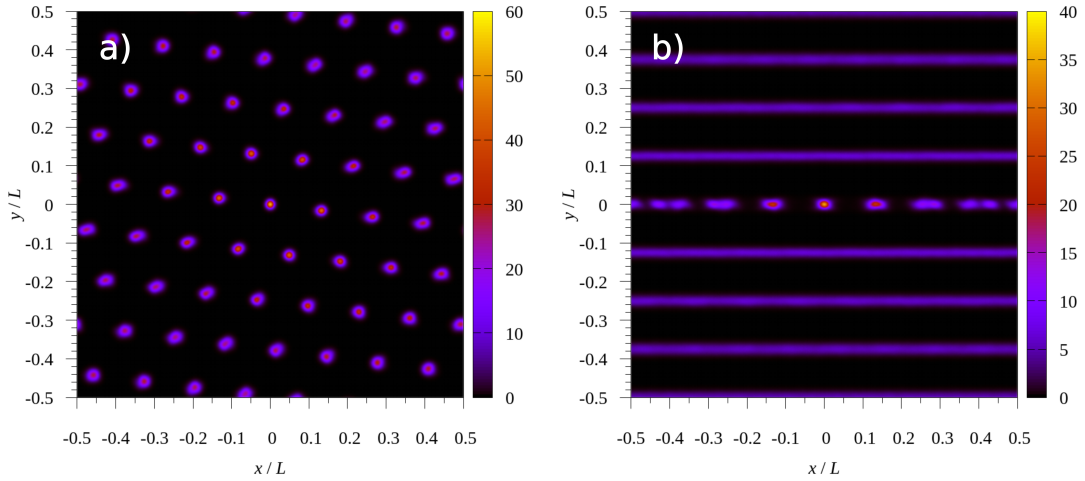

Figure 3.2: Distribution function $g^{(2)}(\mathbf{x})$ for a) $\tilde{U} = 0$ (static case) and b) $\tilde{U} = 15$. In both cases, $\tilde{D} = 0.015$, $R = 0.1L$. Note the different colour scales between the plots.

The separation between channels seems to be independent of $\tilde{U}$ for the range of values under study (compare the last snapshot of Fig.3.1b)–d)), and to be around $\Delta y \simeq 1.25R/L$. The separation between clusters is of order $a^U \sim 1.3R/L$. These two scales are very similar to $a^0 \simeq 1.4R/L$, which seems to indicate that the presence of the flow does not alter greatly the critical wavelength of the emergent pattern over the homogeneous distribution, although it introduces a preferred direction. We will attempt to explain this results in Sec. 3.4. Meanwhile, let us turn our attention to the role of the diffusion.

3.2 Cluster formation dependence on $\tilde{D}$

In Ref. [4] it was shown that, for the static case, the critical value of the diffusion coefficient, for the particular choice of GEM-3 potential used in this work, is $\tilde{D}_c^0 = 0.0823$. Above this value, there is no negative Fourier mode of the potential that can overcome the diffusion and therefore there is no stable pattern formation in the static case.

Maintaining $\tilde{U} = 3$ and $R = 0.1L$ as before, we study the system for different increasing values of $\tilde{D}$ to see if the mode coupling of the horizontal modes affects the critical value of $\tilde{D}$. Plots of non-equilibrium steady states are shown in Fig. 3.3. As expected, the growth of $\tilde{D}$ makes that the compact clusters of our original case $\tilde{D} = 0.015$, Fig. 3.3a), spread out, Fig. 3.3b), until we get near the critical value $\tilde{D}_c^0$, Fig. 3.3c), where only certain areas still have some diluted clusters. Above $\tilde{D}_c^0$, Fig. 3.3d), any trace of a clustering region is washed out as the system evolves.

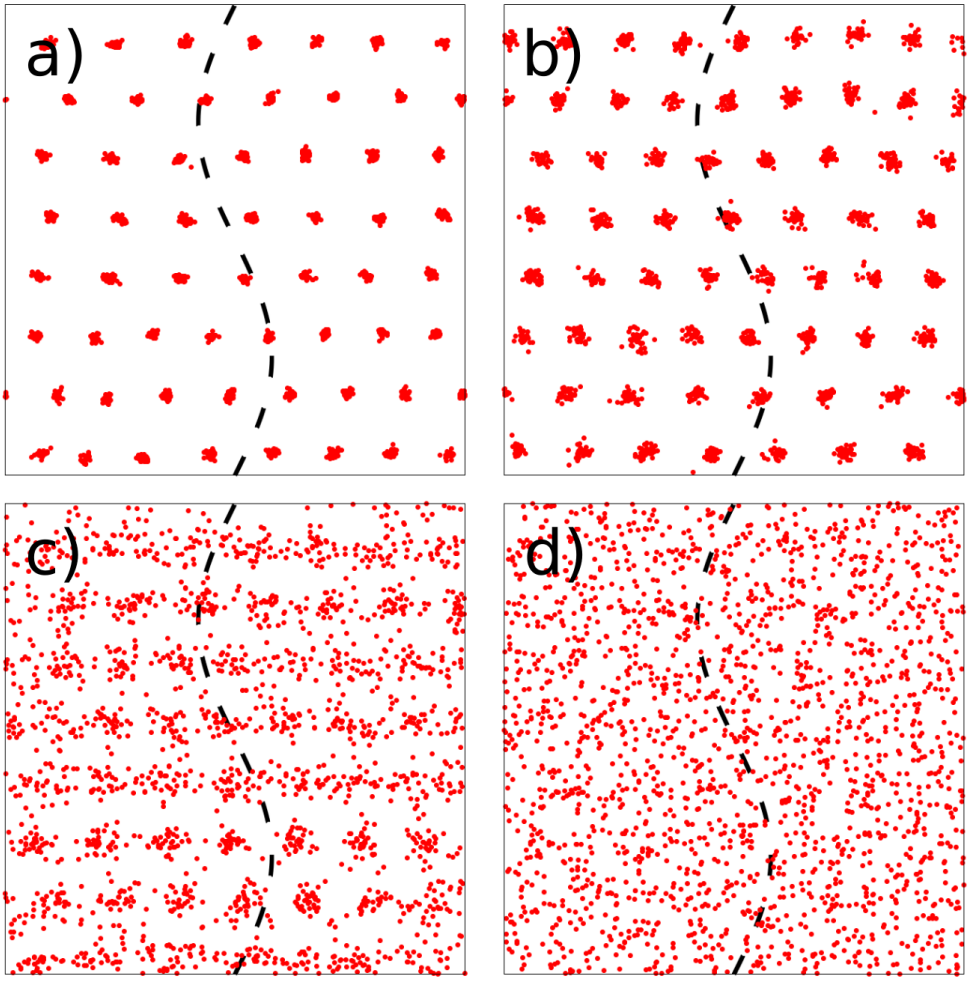

Figure 3.3: Snapshots for different values of $\tilde{D}$: a) $\tilde{D} = 0.015$, b) $\tilde{D} = 0.0375$, c) $\tilde{D} = 0.075$, d) $\tilde{D} = 0.1125$. Superimposed dashed curves are the sine-flow profile. Amplitude as the one for $\tilde{U} = 3$ in Fig. 3.1c).

Although the clusters widen as $\tilde{D}$ increases, even the disperse ones of Fig. 3.3c) appear in channels. In Fig. 3.4 we show the particle distribution $g^{(2)}(\mathbf{x})$ for the

values of $\tilde{D}$ of Fig. 3.3. It is clear that the spreading of clusters due to the diffusion hinders their formation, since particles can diffuse in the vertical direction and jump between channels, as signalled by the non-zero population between channels in Fig. 3.4c). This stands in contrast with increasing $\tilde{U}$, which enhances the formation of channels, as shown previously in Fig. 3.2, trapping the particles in them, but not affecting the cluster formation in the long-term limit, Fig. 3.2d). However, the channels are still present even when $\tilde{D} \sim \tilde{D}_c^0$, separated by the same distance as before. Above $\tilde{D}_c^0$, Fig. 3.4d), the pattern disappears and the system remains homogeneous. This implies that the critical value of $\tilde{D}$ should be close to that of the static case, $\tilde{D}_c^U \simeq \tilde{D}_c^0$. We will try to explain why in Sec. 3.4 below.

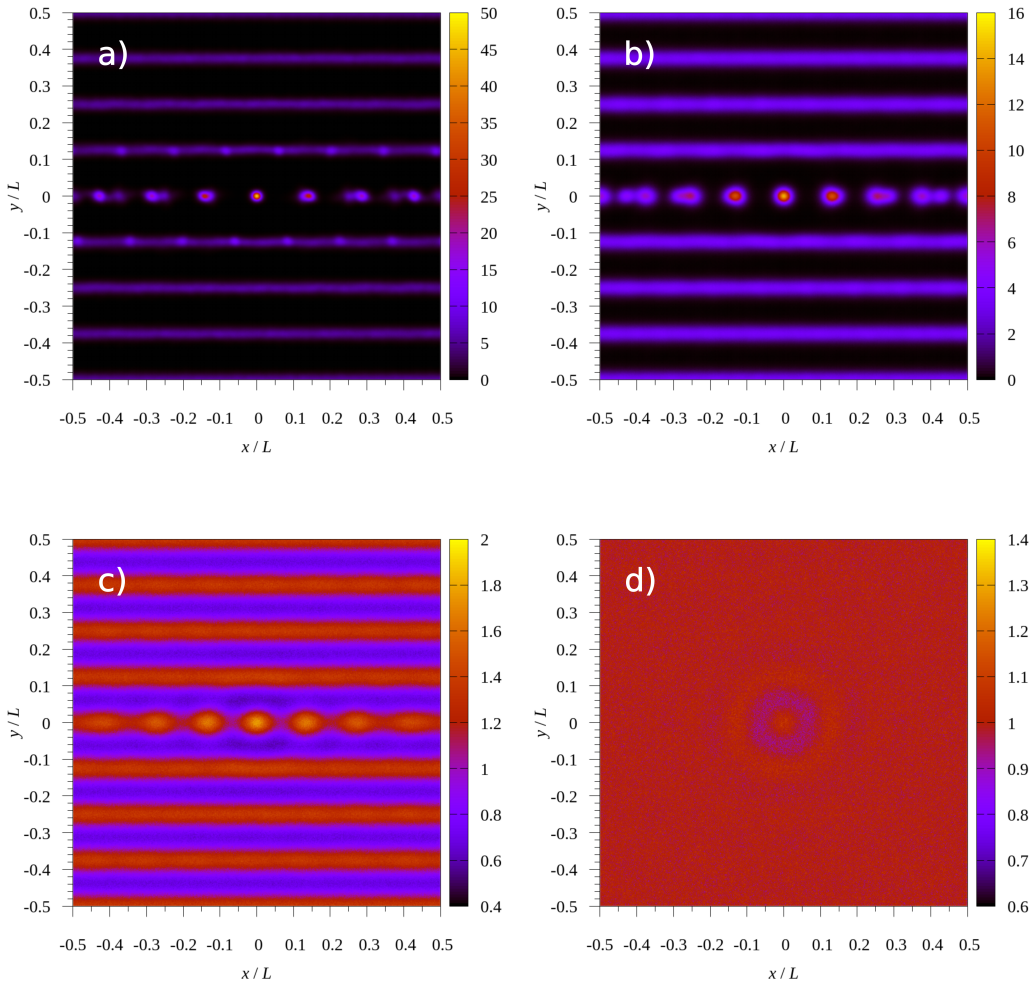

Figure 3.4: Particle distribution $g^{(2)}(\mathbf{x})$ for different values of $\tilde{D}$: a) $\tilde{D} = 0.015$, b) $\tilde{D} = 0.0375$, c) $\tilde{D} = 0.075$, d) $\tilde{D} = 0.1125$. Note the different colour scales between the plots.

3.3 Periodicity dependence on R

Before going into the justification of the above results, we now proceed to study what happens when the interaction length R is changed. We have seen that the separation between channels seems to be rather insensitive to the values of $\tilde{U}$ and $\tilde{D}$ (if $\tilde{D} < \tilde{D}_c$), and to be around $\Delta y \simeq 1.25R/L$. Therefore, we expect that changing R will affect the number of channels present in the cell. We will maintain the values $\tilde{D} = 0.015$ and $\tilde{U} = 3$ fixed, therefore studying a system of similar characteristics to the one showed above in Fig. 3.1c).

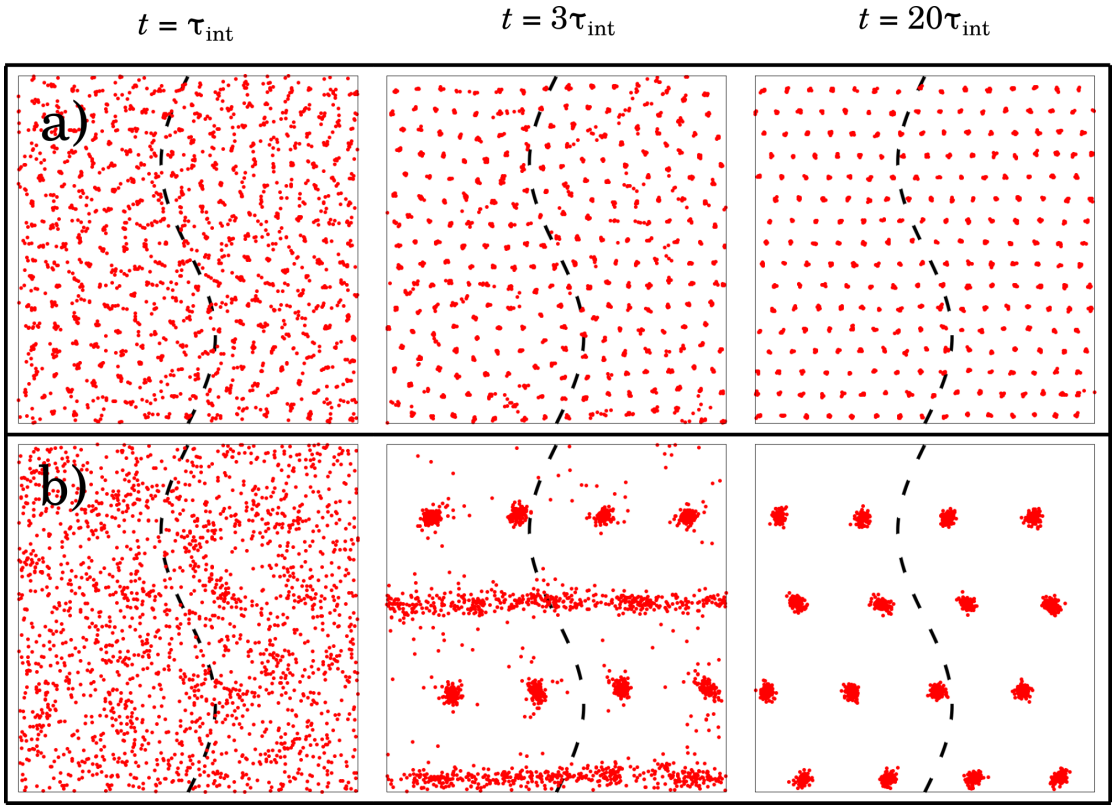

Figure 3.5: Particle configurations at different times for different interaction lengths: a) $R = 0.05L$, b) $R = 0.2L$. In both cases, $\tilde{U} = 3$ and $\tilde{D} = 0.015$. Superimposed dashed curves represent the sine-flow profile, as before.

Typical snapshots are presented in Fig. 3.5 for $R = 0.05L$ (upper row) and $R = 0.2L$ (bottom row). The smaller interaction length in Fig. 3.5a), $R << L$ permits the earlier formation of small clusters that are not distorted, but only organized by the external flow as time goes on to generate the channels. As R is

increased and $R \lesssim L$, the clusters are less but more populated, thus wider, and the shear affects them easier as seen in Fig. 3.5b), second snapshot. Clusters are formed where the flow is maximum and only channels are visible where it is zero. Therefore, the ratio $\tilde{k} \equiv R/L = \tilde{q}/2\pi$ seems to have a role on the short term dynamics of the generation of the structures, albeit the long-term non-equilibrium steady state is the same as before.

The corresponding distributions $g^{(2)}(\mathbf{x})$ are shown in Fig. 3.6. It is clear that changing by a factor of 2 the interaction length R modifies accordingly the number of channels present in the distributions. From the images, it is easy to see that for $R = 0.05L$, $\Delta y \simeq 0.0625 = 1.25R/L$ and for $R = 0.2L$, $\Delta y \simeq 0.25 = 1.25R/L$. For the case $R = 0.05L$, from the central channel of Fig. 3.6a), it is seen as before that channels do not have the same number of clusters and therefore these appear blurred in this averaged distribution. They have between and 14 and 16 clusters, around the double of the number of clusters in the $R = 0.1L$ case discussed earlier, whereas for $R = 0.2L$ each channel has 4 clusters (half the population of the $R = 0.1L$ case) which appear undistorted in the average.

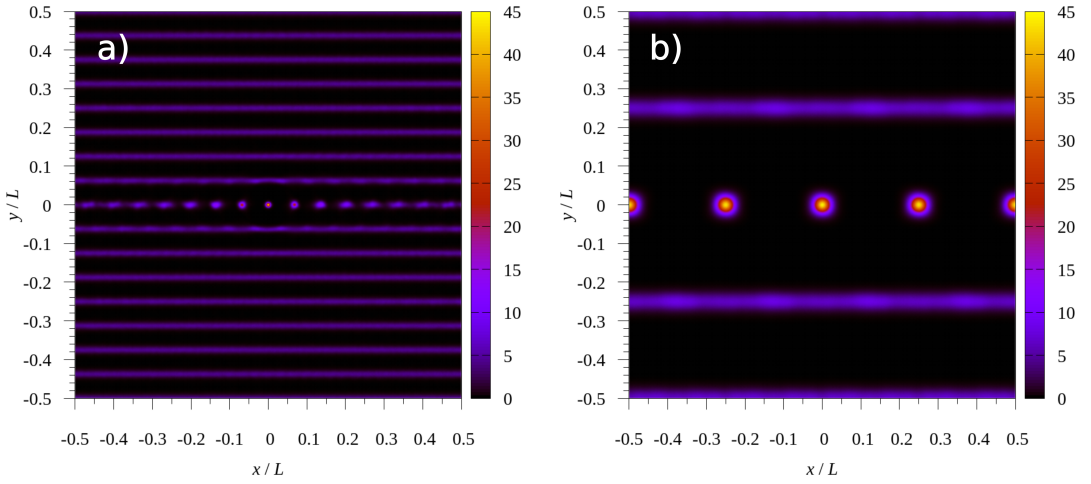

Figure 3.6: Distribution function $g^{(2)}(\mathbf{x})$ for a) $R = 0.1L$ and b) $R = 0.05L$. In both cases $\tilde{U} = 3$ and $\tilde{D} = 0.015$.

3.4 Linear stability analysis

We have seen that our system generates a spatiotemporal pattern with stable, static channels in the transversal direction with respect to the flow, formed by groups of clusters that move with a common velocity following the flow. The distance between channels Δy and the distance between clusters are of the order of the lattice constant a^0 of the static case. Moreover, Δy seems to depend mainly on R and to be independent of the flow amplitude $\tilde{U}$ and the value of the diffusion coefficient $\tilde{D}$. Besides, the critical value of the diffusion appears to be very similar to the critical value of the static case, $\tilde{D}_c^U \simeq \tilde{D}_c^0$.

To explain qualitatively these properties of the pattern that appears over the (dimensionless) uniform density scenario $\rho(\mathbf{x}, t) = 1$, we study the Dean-Kawasaki equation (2.20) derived in 2.2 taking a small perturbation $\delta\rho(\mathbf{x}, t)$ such that $\rho(\mathbf{x}, t) = 1+\delta\rho(\mathbf{x}, t)$. We are not going to use the full stochastic equation, but instead we will study its deterministic counterpart, which is obtained by averaging over noise realizations [1]. We therefore work with the density $\rho = \langle\tilde{\rho}\rangle$, where the average is over noise realizations, with the further mean-field approximation that $\langle\tilde{\rho}(\mathbf{x}, t)\tilde{\rho}(\mathbf{x}', t)\rangle \approx \rho(\mathbf{x}, t)\rho(\mathbf{x}', t)$ [1, 4].

Used the perturbed form of $\rho(\mathbf{x}, t)$ and neglecting terms of order $\delta\rho^2$, we get the linearized, deterministic equation

$$\partial_t\,\delta\rho(\mathbf{x}, t) + \tilde{U}\sin(\tilde{q}y)\partial_x\,\delta\rho(\mathbf{x}, t) = \tilde{D}\nabla^2\delta\rho(\mathbf{x}, t) + \nabla^2\left[\int d\mathbf{x}'\tilde{V}(|\mathbf{x}' - \mathbf{x}|)\delta\rho(\mathbf{x}', t)\right]. \tag{3.2}$$

Since we are dealing with an equation with periodic coefficients, we use the Floquet decomposition

$$\delta\rho_{\mathbf{k}}(\mathbf{x}, t) = \mathrm{e}^{i\mathbf{k}\cdot\mathbf{x}+\lambda(\mathbf{k})t}\sum_n C_n(\mathbf{k})\mathrm{e}^{in\tilde{q}y}, \tag{3.3}$$

to investigate the dynamics of a wavevector $\mathbf{k}$. In particular, our aim is to find the form of the growth rate $\lambda(\mathbf{k})$ to obtain those modes that will grow over the homogeneous steady state, i.e., those with $\Re\{\lambda(\mathbf{k})\} > 0$.

Substituting in (3.2), the first and third terms can be directly computed:

$$\partial_t \, \delta\rho_{\mathbf{k}}(\mathbf{x},t) = \mathrm{e}^{i\mathbf{k}\cdot\mathbf{x}+\lambda(\mathbf{k})t} \sum_n \lambda(\mathbf{k}) C_n(\mathbf{k}) \mathrm{e}^{in\tilde{q}y}, \tag{3.4}$$

$$\begin{aligned} \tilde{D}\nabla^2 \delta\rho_{\mathbf{k}}(\mathbf{x},t) &= -\mathrm{e}^{i\mathbf{k}\cdot\mathbf{x}+\lambda(\mathbf{k})t} \sum_n \tilde{D}\left[k_x^2 + (k_y + n\tilde{q})^2\right] C_n(\mathbf{k}) \mathrm{e}^{in\tilde{q}y} = \\ &= -\mathrm{e}^{i\mathbf{k}\cdot\mathbf{x}+\lambda(\mathbf{k})t} \sum_n \tilde{D} p_n^2 C_n(\mathbf{k}) \mathrm{e}^{in\tilde{q}y}, \end{aligned} \tag{3.5}$$

where we have introduced $\mathbf{p}_n \equiv \mathbf{k} + n\mathbf{q} \equiv (k_x, k_y + n\tilde{q})$. The integral term can be written in terms of the Fourier transform of the potential, $\hat{V}(k)$, as

$$\begin{aligned} \nabla^2 \left[\int d\mathbf{x}' \tilde{V}(\mathbf{x}') \delta\rho(\mathbf{x}'+\mathbf{x},t) \right] &= \nabla^2 \left[\sum_n C_n(\mathbf{k}) \mathrm{e}^{in\tilde{q}y} \mathrm{e}^{i\mathbf{k}\cdot\mathbf{x}+\lambda(\mathbf{k})t} \int d\mathbf{x}' \tilde{V}(\mathbf{x}') \mathrm{e}^{i\mathbf{p}_n\cdot\mathbf{x}} \right] = \\ &= -\mathrm{e}^{i\mathbf{k}\cdot\mathbf{x}+\lambda(\mathbf{k})t} \sum_n p_n^2 \hat{V}(p_n) C_n(\mathbf{k}) \mathrm{e}^{in\tilde{q}y}, \end{aligned} \tag{3.6}$$

noting that $\tilde{V}(\mathbf{x})$ only depends on the modulus of $\mathbf{x}$. Finally, the second term of (3.2) can be computed expanding the sine and renaming the index n inside the summation:

$$\begin{aligned} \frac{\tilde{U}}{2i}\left(\mathrm{e}^{i\tilde{q}y} - \mathrm{e}^{-i\tilde{q}y}\right) \partial_x \delta\rho_{\mathbf{k}}(\mathbf{x},t) &= \frac{1}{2}\tilde{U}k_x \mathrm{e}^{i\mathbf{k}\cdot\mathbf{x}+\lambda(\mathbf{k})t} \sum_n C_n(\mathbf{k}) \left(\mathrm{e}^{i\tilde{q}y} - \mathrm{e}^{-i\tilde{q}y}\right) \mathrm{e}^{in\tilde{q}y} = \\ &= -\frac{1}{2}\tilde{U}k_x \mathrm{e}^{i\mathbf{k}\cdot\mathbf{x}+\lambda(\mathbf{k})t} \sum_n \left[C_{n+1}(\mathbf{k}) - C_{n-1}(\mathbf{k})\right] \mathrm{e}^{in\tilde{q}y}. \end{aligned} \tag{3.7}$$

Collecting terms, the equation now reads

$$\mathrm{e}^{i\mathbf{k}\cdot\mathbf{x}+\lambda(\mathbf{k})t} \sum_n \left\{ \left[\lambda(\mathbf{k}) + p_n^2\left(\tilde{D} + \hat{V}(p_n)\right)\right] C_n(\mathbf{k}) - \frac{1}{2}\tilde{U}k_x \left[C_{n+1}(\mathbf{k}) - C_{n-1}(\mathbf{k})\right] \right\} \mathrm{e}^{in\tilde{q}y} = 0, \tag{3.8}$$

and hence we obtain a coupled linear system for the coefficients $C_n(\mathbf{k})$,

$$\left[\lambda(\mathbf{k}) + p_n^2\left(\tilde{D} + \hat{V}(p_n)\right)\right] C_n(\mathbf{k}) = \frac{1}{2}\tilde{U}k_x \left[C_{n+1}(\mathbf{k}) - C_{n-1}(\mathbf{k})\right]. \tag{3.9}$$

We shall not pursue a complete solution of these coupled equations. However, we can still gain some insight on why the periodicities that appear in our system resemble those of the case without flow.

To see how we can reduce this system to some simpler cases, let us firstly note that in the case $\tilde{U} = 0$ we shall recover the static solution as obtained by Delfau *et al.* in Ref. [4]. Equation (3.9) in this case reads

$$\left[\lambda(\mathbf{k}) + p_n^2 \left(\tilde{D} + \hat{V}(p_n)\right)\right] C_n(\mathbf{k}) = 0 \tag{3.10}$$

but since the p_n with $n \neq 0$ includes a explicit reference to $\mathbf{q}$, we have to set $C_n(\mathbf{k}) = 0$ for all $n \neq 0$. The perturbation $\delta\rho$ represents a Fourier mode with growth rate

$$\lambda^{stc}(\mathbf{k}) = -k^2 \left[\tilde{D} + \hat{V}(k)\right] \tag{3.11}$$

which is the desired expression for the static case [4]. As mentioned earlier, this expression predicts that stable patterns will grow only if the negative values of $\hat{V}(k)$ overcome the diffusion, which will be possible only if $\tilde{D} < \tilde{D}_c^0 = 0.0823$ (for the GEM-3 potential in the static case). This last value corresponds to $\tilde{D}_c^0 = -\min\{\hat{V}(k)\}$. The first modes to grow will have $k = k_c^0 = 5.0$, corresponding to a critical value for the lattice constant of $a^0 = 1.44$ [4]. Modes with positive $\hat{V}(k)$ will have negative growth rates and will not be stable, hence the need for a negative part in $\hat{V}(k)$.

Since the $n = 0$ term defines the static case, in the presence of weak coupling, $\tilde{U} << 1$, we can add in a first approximation the modes corresponding to $n = \pm 1$, which have the periodicity of the flow. Hence, we impose $C_n = 0$ for $|n| > 1$. Defining

$$A_n \equiv p_n^2 \left(\tilde{D} + \hat{V}(p_n)\right), \qquad B \equiv \tilde{U} k_x/2, \tag{3.12}$$

for notation brevity, the remaining system reads

$$\begin{pmatrix} \lambda(\mathbf{k}) + A_{-1} & -B & 0 \\ B & \lambda(\mathbf{k}) + A_0 & -B \\ 0 & B & \lambda(\mathbf{k}) + A_{+1} \end{pmatrix} \begin{pmatrix} C_{-1} \\ C_0 \\ C_{+1} \end{pmatrix} = \mathbf{0}. \tag{3.13}$$

This is a homogeneous system, which will only be solvable if the determinant of the coefficient matrix is zero. Therefore, the growth rate $\lambda(\mathbf{k})$ has to satisfy

$$\left(\lambda(\mathbf{k}) + A_0\right)\left(\lambda(\mathbf{k}) + A_{-1}\right)\left(\lambda(\mathbf{k}) + A_{+1}\right) = -2B^2 \left(\lambda(\mathbf{k}) + \frac{A_{-1} + A_{+1}}{2}\right). \tag{3.14}$$

In principle, this equation will give three solutions for $\lambda(\mathbf{k})$, of which two may be complex conjugates. If $\lambda(\mathbf{k})$ is complex, its real part will give the growth rate of the corresponding mode, while its imaginary part will add a temporal modulation to the pattern.

We expect, from the results of the simulations shown previously in Sec.3.1, that in this approximation $k_c^U \approx k_c^0$. Recalling that $\mathbf{p}_{\pm 1} = \mathbf{k} \pm \mathbf{q}$, and since with our reference parameters $\tilde{q} = 0.2\pi \simeq 0.63 << k_c^0$, expanding $A_{\pm 1}$ in Taylor series we get

$$A_{\pm 1}(\mathbf{k}) = A_0(\mathbf{k} \pm \mathbf{q}) \approx A_0(\mathbf{k}) \pm \tilde{q}\,\frac{\partial A_0}{\partial k_y}(\mathbf{k}) + \frac{1}{2}\tilde{q}^2 \frac{\partial^2 A_0}{\partial k_y^2}(\mathbf{k}) + \mathcal{O}(q^3). \tag{3.15}$$

For convenience, we define $[\partial^n A_0] \equiv \partial^n A_0 / \partial k_y^n$. Substituting in eq.(3.14) and neglecting terms in $\tilde{q}^4$ and $\tilde{U}^2\,\tilde{q}^2$, we get the simpler expression

$$(\lambda(\mathbf{k}) + A_0)\left\{ \left(\lambda(\mathbf{k}) + A_0 + \frac{1}{2}\tilde{q}^2\left[\partial^2 A_0\right]\right)^2 - \tilde{q}^2\left[\partial A_0\right]^2 \right\} = -2B^2\,(\lambda(\mathbf{k}) + A_0) \tag{3.16}$$

from which we recover the static solution

$$\lambda^0(\mathbf{k}) = -A_0 = -k^2\left[\tilde{D} + \hat{V}(k)\right] = \lambda^{stc}(\mathbf{k}), \tag{3.17}$$

and two new branches appear,

$$\begin{aligned} \lambda^{\pm}(\mathbf{k}) &= -A_0 - \frac{1}{2}\tilde{q}^2\left[\partial^2 A_0\right] \pm \sqrt{\tilde{q}^2\left[\partial A_0\right]^2 - 2B^2} = \\ &= \lambda^{stc}(\mathbf{k}) - \frac{1}{2}q^2\left[\partial^2 A_0\right] \pm \sqrt{\tilde{q}^2\left[\partial A_0\right]^2 - \frac{1}{2}\tilde{U}^2 k_x^2}. \end{aligned} \tag{3.18}$$

Let us discuss two particular cases for these new solutions. Firstly, when $k_x = 0$ (corresponding to purely transversal modes), we recover

$$\lambda^{\pm}(0, k_y) = -\left(A_0 \pm \tilde{q}\left[\partial A_0\right] + \frac{1}{2}\tilde{q}^2\left[\partial^2 A_0\right]\right) = -A_{\pm 1}(k_y) = -A_0(k_y \pm \tilde{q}) \tag{3.19}$$

which are the correct solutions in these case, as seen from the original equation (3.9) when $B = 0$. These modes produce the same behaviour as the static ones, but with their critical wavevectors slightly displaced, $k_c^U = k_c^0 \pm \tilde{q}$. These branches of solutions will compete with the original to finally promote the apparition of the

(static) spatial periodicity in the transversal direction with $\Delta y \lesssim a^0$ that we saw in the simulations of previous sections. The flow strength $\tilde{U}$ does not play a role in this selection, and the critical value of the diffusion coefficient is the same as in the static case, $\tilde{D}_c^U = \tilde{D}_c^0$, for these modes.

Secondly, when $k_y = 0$ (purely longitudinal modes), since we are only concerned with modes $k_x \simeq k_c^0 >> \tilde{q}$, to first order we have

$$\lambda^{\pm}(k_x, 0) \simeq -\left[A_0 + \frac{1}{2}\tilde{q}^2\left[\partial^2 A_0\right]\right] \pm i\,\frac{1}{\sqrt{2}}\tilde{U}|k_x|\left[1 - \left(\frac{q\left[\partial A_0\right]}{\tilde{U}k_x}\right)^2\right] \approx$$
$$\approx -A_0 \pm i\,\frac{1}{\sqrt{2}}\tilde{U}|k_x| + \mathcal{O}(\tilde{q}^2). \tag{3.20}$$

The real part of $\lambda^{\pm}(k_x, 0)$ have the same form as above and will promote similar periodicities but, moreover, their imaginary parts will introduce a temporal modulation to produce travelling waves with velocity $\tilde{U}/\sqrt{2}$ in the longitudinal direction.

More general modes will share characteristics with one or the other case depending on the value of the square root in $\lambda^{\pm}(\mathbf{k})$ of equation (3.18). The promoted periodicities in this weak coupling scenario are near those of k_c^0 with corrections of order q at most. The flow strength $\tilde{U}$ only appears as the velocity of the temporal modulation of the patterns, explaining why the inter-channel distance Δy saw in Sec. 3.1, Fig. 3.1 seemed independent of the value of $\tilde{U}$. It seems reasonable to deduce that this temporal modulation in the longitudinal direction introduces the necessary asymmetry that provokes the emergence of the channels. Besides, since in all cases we have a growth rate of the form $\lambda^{stc} = -A_0(\mathbf{k})$, the critical value of $\tilde{D}$ is mostly unchanged, and therefore $\tilde{D}_c^U \approx \tilde{D}_c^0$ as seen in the simulations.

This simple approximation has thus allow us to explain qualitatively the results obtained from the simulations. Needless to say, when $\tilde{U} \sim 1$ or $\tilde{q} \propto R/L \sim 1$ more terms in the expansion are necessary to properly describe the dynamics, as we have seen in Figs. 3.1d) and 3.5b). Nevertheless, no further relevant phenomena have appeared in these cases and the final non equilibrium steady state is essentially the same for the whole range of values studied. Therefore in general terms the above qualitative justification explains the results from the simulations.

Chapter 4

Chaotic flow

Until now we have been focusing solely on the case of steady shear flow. We now briefly discuss the case when we have the alternating sine-flow of equations (2.24)–(2.24) presented in Sec. 2.4, which represents a chaotic mixing flow.

4.1 Cluster formation dependence on T

We have performed simulations of our system with the sine-flow of Fig. 2.1, fixing the reference values $\tilde{U} = 3$, $\tilde{D} = 0.015$ and $R = 0.1L$. The external velocity field acts alternatively in two orthogonal directions during a time interval $T/2$. When applying this type of alternating flow, one has to be careful to avoid the formation of KAM tori [14], since their appearance may complicate the scenario due to the presence of areas of different advective behaviour within the cell. For that reason the phase ϕ of the flow will be a uniform random variable on the interval $[-\pi, \pi]$ that will change its value at the end of each period during the simulations. This ensures that the flow is aperiodic, albeit the presence of diffusion also allows the particles to cross the advective barriers of the bare flow (compare, for instance, Figs. 2.10 and 2.16 of Ref. [14]).

During each $T/2$ interval, the flow profile has the steady form used in Chapter 3, and therefore it is expected that particles will try to order themselves in the channels-of-clusters spatiotemporal pattern shown above. In Fig. 4.1 we have plot-

ted the configurations at $t = (5/2)T$, just before a change of direction, for different values of the period. In Fig. 4.1a) the small value of the period, $T = 0.02 \sim \tau_{int}$ allows the formation of clusters but not of channels. As the flow change its direction, and since its phase changes between periods, the clusters are pushed towards one another, which deforms them. This mechanism is specially strong when two neighbouring clusters are suddenly driven in opposite directions by the flow. Distorted clusters or filaments of particles affect the nearby clusters, and provokes a recombination of particles that try to form new clusters. In the case of strongly mixing flow, $T << \tau_{int}$, clusters will not have enough time to form. In the opposite case, as T grows, this recombination is mostly completed and the channels begin to form, as seen in Fig. 4.1b). It would be interesting to study this recombination of the particles into new clusters, which may be important for chemical reactions and biological processes between particles in a more general model that the one studied here.

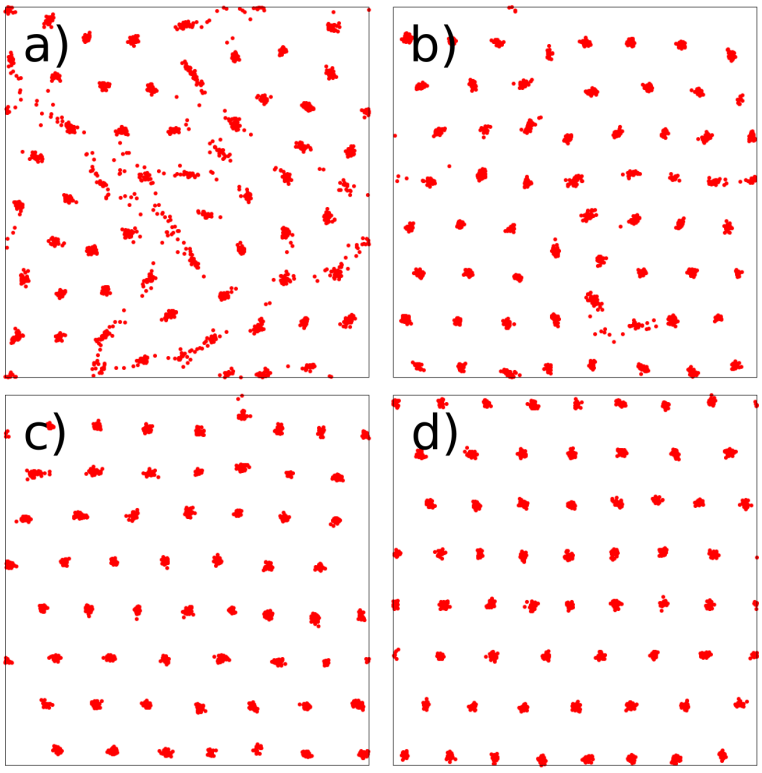

Figure 4.1: Typical snapshots at the middle configuration of a period, $t = (5/2)T$, just before the change of direction, for different values of T: a) $T = 0.02$, b) $T = 0.08$, c) $T = 0.32$, d) Shear flow. In all the simulations, $\tilde{U} = 3$, $\tilde{D} = 0.015$, $R = 0.1L$.

When the period T is much larger than any of the clusters time-scales τ, the pattern will form completely and follow the same dynamics that have been shown above, until the sine-flow changes its direction at $t = T/2 \mod T$ when the particles will reorganize themselves again along the new longitudinal direction, as can be seen comparing Fig. 4.1c), where $T/2 = 0.16 \approx 10\tau_{int}$, to the shear configuration shown in Fig. 4.1d) for comparison.

We can compare up to which point the channels can develop by computing the transversal distribution $h^{(2)}(y)$,

$$h^{(2)}(y) = \frac{1}{N_p} \left\langle \sum_{i=1}^{N} \sum_{j>i} \delta(y - y_{ji}) \right\rangle \tag{4.1}$$

where $y_{ji} = y_j - y_i$ and N_p is the number of possible pairs. It is easy to see that this distribution gives an idea of the average of $g^{(2)}(\mathbf{x})$ along the longitudinal direction.

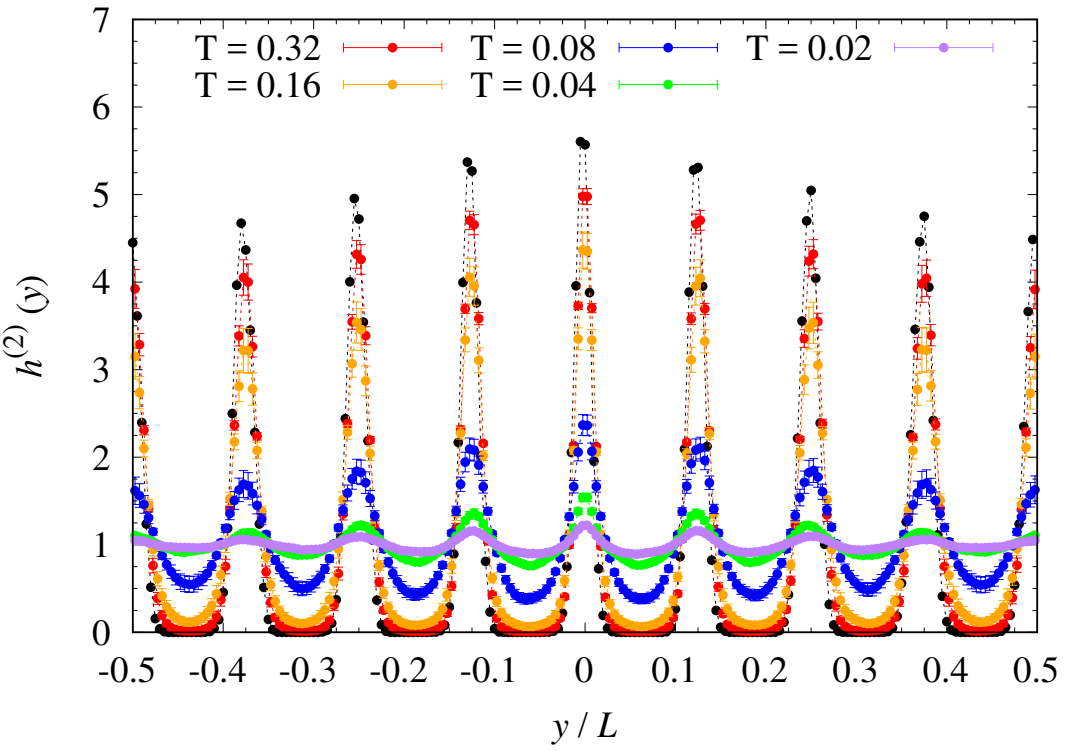

Figure 4.2: Vertical distribution function $h^{(2)}(y)$ for different periods. Black points correspond to the static case for comparison. Error bars represent statistical errors. Dashed lines are guides to the eye.

Performing 20 independent simulations until $t = (5/2)T$ for each T, we have computed $h^{(2)}(y)$ averaging over the final configurations, just before a $T/2$-swift of direction. The resulting distributions are shown in Fig. 4.2. It is clear that the modes growing in the transversal direction are the same as before. From the curves that reach the value zero between peaks, we can infer that the minimum period for the channels to form is around $T \simeq 0.16$. The inter-channel distance is obtained from the separation between peaks, and is $\Delta y \simeq 0.125 = 1.25R/L$. In a sense, we are effectively seen (as T grows) the temporal evolution of $g^{(2)}(\mathbf{x})$, averaged over the longitudinal direction, for the case of shear flow beginning with a random initial condition. Black points correspond to the same average done over an equivalent direction of a stable cluster crystal configuration (without flow), shown for comparison. The difference between Δy and the cluster crystal lattice constant a^0 is negligible.

Chapter 5

Conclusions

In this Master Thesis, we have investigated the effect of an external flow with an ensemble of Brownian particles interacting via a repulsive GEM-3 potential $\tilde{V}(\mathbf{x})$, which in the absence of flow are known to form a cluster crystal if the diffusion is sufficiently low.

We have shown by means of direct simulation of the particles' dynamics that the addition of a external shear flow imposing a velocity field $\tilde{\mathbf{u}}(\mathbf{x}) = \tilde{U}\sin(\tilde{q}y)\hat{\mathbf{e}}_x$, leads to a non-equilibrium steady state of parallel, quasi-1D channels of clusters that move following the flow direction. These channels are separated by a distance $\Delta y \simeq 1.25R/L$, that only depends on the interaction length R and not on the flow intensity $\tilde{U}$ nor on the diffusion coefficient $\tilde{D}$. As $\tilde{D}$ is increased, particles are allowed to move from one channel to another, until a critical value $\tilde{D}_c^U$ is achieved when the diffusion dissolves the pattern and the homogeneous configuration is recovered. The value of $\tilde{U}$ is important when considering the short-term dynamics from an initial random configuration, since it measures the ratio between the interaction and advection time-scales. If $\tilde{U} << 1$ clusters will form rapidly and after a transient period the flow will reorganize the clusters to form the channels. If $\tilde{U} >> 1$ the structure in channels will appear before clusters emerge on top of them. In either case, the long-term spatiotemporal pattern is the same.

The inter-channel distance Δy and the distance between clusters of a particular channel are of the same order and similar to the lattice constant $a_0 = 1.44R/L$

of the static case reported by Delfau *et al.* in Ref. [4]. In the same way, it is seen that the critical value of the diffusion in both cases are essentially the same, $\tilde{D}_c^U \simeq \tilde{D}_c^0 = 0.0823$ [4]. We have been able to explain qualitatively why these quantities are similar with and without flow by pursuing a linear stability analysis of the Dean-Kawasaki equation with the external flow [1,3,5]. We have found that, in the weak coupling approximation, the growth rates $\lambda(\mathbf{k})$ of Floquet modes have essentially the same form as the static one, $\Re\{\lambda(\mathbf{k})\} \approx \lambda^{stc}(\mathbf{k}) = -k^2\left[\tilde{D} + \hat{V}(\mathbf{k})\right]$, where $\hat{V}(\mathbf{k})$ is the Fourier transform of the interaction potential, which explains why $\tilde{D}_c^U \simeq \tilde{D}_c^0$.

Purely transversal modes are static. Their modulus k_c^U of the critical modes that generates the pattern have a correction of order $\tilde{q}$, $k_c^U = k_c^0 \pm q$, which indicates that the spatial periodicities in the system with flow should not be very different from the lattice constant of the static cluster crystal $a_0 = 2\pi/k_c^0$, as we have seen in the simulations. On the contrary, purely transversal modes are dynamic. Their growth rate correspond approximately to the static one, but has a complex phase that creates a temporal modulation of the pattern with velocity $\tilde{U}/\sqrt{2}$ in the longitudinal direction. More general modes share partly these behaviours. The addition of the static modes in the transversal direction plus the dynamic ones in the direction of the flow is the responsible mechanism that generates de channels of clusters that are observed.

In the case of mixing alternating flow, this spatiotemporal pattern is destroyed and recomposed after each change of direction. When T is of the order of the interaction time scale τ_{int} clusters form but channels do not have time to emerge. The clusters are deformed and may form filaments of particles that will try to form new clusters. When $T >> \tau_{int}$, the channels form completely before the new swift of direction, which also produces a recombination of particles to form new clusters.

As further research in the system under study, it would be interesting to investigate the effects of boundaries and hydrodynamic interactions not accounted for in this simple model. The formation of channels may also be important if the

particles present chemical or biological processes that depend on the local density, specially because the alternating flow represents a recombination mechanism which rate can be controlled by the relationship between the flow period T and the interaction time scale τ_{int} in which clusters form.

Bibliography

[1] A. J. Archer and M. Rauscher. Dynamical density functional theory for interacting brownian particles: stochastic or deterministic? *Journal of Physics A: Mathematical and General*, 37(40):9325, 2004.

[2] P. G. de Gennes. Soft matter. *Rev. Mod. Phys.*, 64:645–648, Jul 1992.

[3] D. S. Dean. Langevin equation for the density of a system of interacting langevin processes. *J. Phys. A: Math. Gen.*, 29(24):L613, 1996.

[4] J.-B. Delfau, H. Ollivier, C. López, B. Blasius, and E. Hernández-García. Pattern formation with repulsive soft-core interactions: Discrete particle dynamics and dean-kawasaki equation. *Phys. Rev. E*, 94(4):042120, 2016.

[5] H. Frusawa and R. Hayakawa. On the controversy over the stochastic density functional equations. *Journal of Physics A: Mathematical and General*, 33(15):L155, 2000.

[6] C. Gardiner. *Stochastic Methods: a Handbook for the Natural and Social Sciences*. Springer-Verlag Berlin Heidelberg, fourth edition, 2009.

[7] C. Likos, A. Lang, M. Watzlawek, and H. Löwen. Criterion for determining clustering versus reentrant melting behavior for bounded interaction potentials. *Physical Review E*, 63(3):031206, 2001.

[8] C. N. Likos. Effective interactions in soft condensed matter physics. *Physics Reports*, 348(4-5):267–439, 2001.

[9] C. N. Likos, B. M. Mladek, D. Gottwald, and G. Kahl. Why do ultrasoft repulsive particles cluster and crystallize? analytical results from density-functional theory. *The Journal of chemical physics*, 126(22):224502, 2007.

[10] H. Löwen. Colloidal soft matter under external control. *Journal of Physics: Condensed Matter*, 13(24):R415, 2001.

[11] M. C. Marchetti, J.-F. Joanny, S. Ramaswamy, T. B. Liverpool, J. Prost, M. Rao, and R. A. Simha. Hydrodynamics of soft active matter. *Reviews of Modern Physics*, 85(3):1143, 2013.

[12] B. M. Mladek, D. Gottwald, G. Kahl, M. Neumann, and C. N. Likos. Formation of polymorphic cluster phases for a class of models of purely repulsive soft spheres. *Phys. Rev. Lett.*, 96(4):045701, 2006.

[13] B. M. Mladek, G. Kahl, and C. N. Likos. Computer assembly of cluster-forming amphiphilic dendrimers. *Physical review letters*, 100(2):028301, 2008.

[14] Z. Neufeld and E. Hernández-García. *Chemical and Biological Processes in Fluid Flows: A Dynamical Systems Approach*. Imperial College Press, 2010.

[15] A. Nikoubashman, G. Kahl, and C. N. Likos. Cluster crystals under shear. *Phys. Rev. Lett.*, 107(6):068302, 2011.

[16] R. Toral and P. Colet. *Stochastic numerical methods: an introduction for students and scientists*. John Wiley & Sons, 2014.